



**HAL**  
open science

# Transition from Phononic to Geometrical Mie Modes Measured in Single Subwavelength Polar Dielectric Spheres

Loubnan Abou-Hamdan, Laure Coudrat, Sébastien Bidault, Valentina Krachmalnicoff, Riad Haïdar, Patrick Bouchon, Yannick De Wilde

► **To cite this version:**

Loubnan Abou-Hamdan, Laure Coudrat, Sébastien Bidault, Valentina Krachmalnicoff, Riad Haïdar, et al.. Transition from Phononic to Geometrical Mie Modes Measured in Single Subwavelength Polar Dielectric Spheres. *ACS photonics*, 2022, 9 (7), pp.2295-2303. 10.1021/acsphotonics.2c00273 . hal-03796708

**HAL Id: hal-03796708**

**<https://hal.science/hal-03796708>**

Submitted on 4 Oct 2022

**HAL** is a multi-disciplinary open access archive for the deposit and dissemination of scientific research documents, whether they are published or not. The documents may come from teaching and research institutions in France or abroad, or from public or private research centers.

L'archive ouverte pluridisciplinaire **HAL**, est destinée au dépôt et à la diffusion de documents scientifiques de niveau recherche, publiés ou non, émanant des établissements d'enseignement et de recherche français ou étrangers, des laboratoires publics ou privés.

# Transition from Phononic to Geometrical Mie Modes Measured in Single Subwavelength Polar Dielectric Spheres

Loubnan Abou-Hamdan,<sup>†,‡</sup> Laure Coudrat,<sup>†</sup> Sébastien Bidault,<sup>†</sup> Valentina Krachmalnicoff,<sup>†</sup> Riad Haïdar,<sup>‡</sup> Patrick Bouchon,<sup>\*,‡</sup> and Yannick De Wilde<sup>\*,†</sup>

<sup>†</sup>*Institut Langevin, ESPCI Paris, PSL University, CNRS, 1 rue Jussieu, F-75005 Paris, France*

<sup>‡</sup>*DOTA, ONERA, Université Paris-Saclay, F-91123 Palaiseau, France*

E-mail: [patrick.bouchon@onera.fr](mailto:patrick.bouchon@onera.fr); [yannick.dewilde@espci.fr](mailto:yannick.dewilde@espci.fr)

## Abstract

Spherical dielectric resonators are highly attractive for light manipulation, thanks to their intrinsic electric and magnetic resonances. Here, we present measurements of the mid-infrared far-field thermal radiation of single subwavelength dielectric spheres deposited on a gold substrate, of radii ranging from 1 to 2.5  $\mu\text{m}$ , which agree quantitatively with simulated absorption cross-sections. For  $\text{SiO}_2$  microspheres, we evidence the excitation of both surface phonon-polariton (SPhP) modes and geometrical electric and magnetic Mie modes. The transition from a phonon-mode-dominated to a Mie-mode-dominated emission spectrum is observed, with a threshold radius of  $\sim 1.5 \mu\text{m}$ . We also show that the presence of the metallic substrate augments the computed spheres' absorption cross-section due to increased local field enhancement, arising from the near-field interaction of the sphere's oscillating charges with their image in the metallic mirror. In contrast, measurements of single subwavelength SPhP-inactive PTFE spheres

reveal that the mid-infrared response of such lossy spheres is dominated by their bulk absorption. Our results demonstrate how engineering the geometrical and dielectric properties of subwavelength scatterers can enable the control of thermal emission near room temperature, with exciting perspectives for applications such as radiative cooling.

Keywords: Thermal emission, spectroscopy, subwavelength spheres, infrared, phonon-polaritons, Mie modes

## Introduction

Dielectric resonators have recently emerged as an alternative to various plasmonic antennas.<sup>1,2</sup> This is mainly due to the fact that dielectric antennas feature, generally in the near-infrared, both electric and magnetic resonances, and exhibit less losses than their plasmonic counterparts, particularly in the visible spectral range.<sup>1-8</sup> The geometrical electrical and magnetic Mie modes supported by high-refractive-index dielectric subwavelength particles, such as Si nanospheres, have been studied extensively at visible and near-infrared wavelengths.<sup>9-11</sup> In the mid-infrared (mid-IR), absorbing dielectric resonators, such as polar dielectric SiO<sub>2</sub> microspheres, have been used in a wide variety of applications, most notably for radiative cooling.<sup>12-17</sup> Their emissivity is indeed high in the mid-IR atmospheric transparency window, while they scatter light with very little absorption at visible and near-infrared wavelengths, where the solar spectrum is prominent.

For such applications, tailoring the individual infrared radiative properties of these dielectric resonating microspheres is of crucial importance for enhancing radiative cooling efficiency. Microspheres are typically self-assembled on a substrate or within a matrix. Most studies aiming at modeling the optical response of such randomized metamaterials are restricted to low particle densities, and make use of effective medium theory calculations.<sup>12,18,19</sup> Both the inter-particle interactions and the presence of a large and extended thermal radiation background in the mid-IR, generally preclude the measurement of the intrinsic mid-IR thermal

radiation properties of single dielectric microspheres.

In this paper, we report the first investigation of the mid-IR thermal radiation of single subwavelength (sub- $\lambda$ ) SiO<sub>2</sub> microspheres supporting surface phonon-polariton (SPhP) modes, using infrared spatial modulation spectroscopy (IR-SMS).<sup>20,21</sup> For comparison, we also present, using the same method, thermal radiation spectra of highly absorbing mid-IR microspheres, made up of an SPhP-inactive material, namely polytetrafluoroethylene (PTFE).

## Results and discussion

To be able to measure the thermal radiation spectra of single microspheres, we place them on a gold substrate, which has the advantage of having a low emissivity at infrared wavelengths while acting as a mirror, directing the emitted radiation in the half-space where the collection optics are located (see Fig. 1 (a)). We note here that this situation is of interest for radiative cooling applications where a metallic mirror is often used as a substrate for reflectivity enhancement.<sup>12-14</sup>

A solution of commercially available SiO<sub>2</sub> microspheres (Sigma Aldrich), of known size, is diluted and deposited on a 100 nm thick gold substrate (see supplementary information, Methods section, for sample preparation). The sample is first examined with a visible microscope to determine the positions of single spheres (see Figs. 1 (b)-(e), insets). The far-field thermal radiation of the selected single spheres is then measured using IR-SMS.

As illustrated in Fig. 1 (a), the sphere's modes are excited thermally by raising the overall temperature of the sample above the thermal bath, to around  $T^* = 440$  K, via a hot plate. The emitted thermal radiation is then collected from the sample using a Cassegrain objective (NA=0.5), which has a conic collection—except for a blind solid angle around the optical axis due to the presence of a secondary mirror. The collected radiation then passes through a step-scan operated Fourier transform infrared (FTIR) spectrometer before reaching a liquid-

nitrogen-cooled mercury cadmium telluride (MCT) detector, enabling the measurement of a thermal radiation spectrum.

As the sample surface is isothermal, the thermal radiation signal at the detector is dominated by an overwhelming background produced by the regions surrounding the microsphere located within a detection area of  $\sim 1000 \mu\text{m}^2$ , which is optically conjugated with the MCT detector. To filter out this background, the sample is modulated laterally with an amplitude of  $\sim 25 \mu\text{m}$ , at a frequency  $\Omega$ , by means of a piezoelectric translation stage. This induces a spatial dependence on the signal contribution coming from the single sphere, as its position oscillates within the detection area. We extract this contribution through lock-in detection, by demodulating the detected signal at the frequency  $\Omega$ , or at a higher harmonic, eliminating the large background.

The IR-SMS spectra of spheres of radii ranging from  $r_o = 1$  to  $2.5 \mu\text{m}$  are shown in Figs. 1 (b)-(e). The measurements show a prominent peak near  $1130 \text{ cm}^{-1}$  for the smallest sphere measured (Fig. 1 (b)), which vanishes as the sphere radius increases above  $1 \mu\text{m}$  (Figs. 1 (c)-(e)), and is supplemented by a new predominant peak, near  $1040 \text{ cm}^{-1}$ , below the transverse optical phonon frequency ( $\omega_{TO}$ ) of  $\text{SiO}_2$ .

The signal measured at the detector,  $S_{\text{sphere}}(\omega, T^*)$ , corresponds to the spectral radiance emitted by the sphere, multiplied by the instrumental response.<sup>22</sup> To remove any temperature or instrumental dependence, we normalize the measured signal with the response of a blackbody sample at the same temperature,  $S_{\text{BB}}(\omega, T^*)$ , measured with the same optical path. The normalized signal,  $S_{\text{norm}}(\omega) = S_{\text{sphere}}(\omega, T^*)/S_{\text{BB}}(\omega, T^*)$ , corresponds to the normalized thermal emission of the single sphere, which, by Kirchhoff's law,<sup>23</sup> is comparable to the absorption cross-section ( $C_{\text{abs}}$ ) of the sphere on the gold substrate.<sup>20,21,24,25</sup>

This normalization procedure is based on the assumption that the sphere and substrate are thermalized to the hot plate temperature (440 K). Due to the inherently small contact area between the sphere and substrate,<sup>26</sup> we have assessed the possibility of a thermal gradient arising within the sphere as a consequence of conductive cooling through air and the sphere

(see Supplementary Information subsection 1.2.2). We find that the sphere temperature deviates by less than 1 K from the substrate temperature, thus validating our assumption.

Previous studies have considered the problem of scattering by a sphere on a substrate analytically. Nevertheless, simple analytical solutions exist only for limited cases, such as a sphere replaced by electric and magnetic dipoles at its center<sup>10,27,28</sup> or for a perfectly electrically conducting substrate.<sup>29,30</sup> We also note that calculating the thermal emission of a macroscopic sphere close to a substrate requires the framework of fluctuational electrodynamics and the discrete dipole approximation.<sup>31</sup> As mentioned above, however, it can be evaluated reciprocally by determining its absorption.<sup>24</sup> In an effort to quantitatively model our results, including the effect of the gold substrate, we performed finite element method (FEM) simulations (Comsol Multiphysics) of the absorption cross-section of the solitary SiO<sub>2</sub> sphere on a gold surface (Figs. 1 (b)-(e), dotted curves). The advantage of this approach is two-fold; it allows one to solve for the full electromagnetic field within the considered geometry while precisely taking into account all the geometrical and material properties of our samples—most notably the dielectric function of the gold substrate—without any approximations. For an accurate representation of the angular interval in which emission from our sample is collected by the Cassegrain objective used in the measurements, we simulated the absorption cross-section of the sphere on gold for unpolarized light impinging at various angles from 10 to 30° (measured from the normal to the Au substrate), and averaged the resulting spectra (see supplementary information, Fig. S1, for the corresponding angle-resolved spectra), which provides a good fit with the measurements (cf. Figs. 1 (b)-(e), solid and dotted curves).

Interestingly, the simulations show that very high absorption cross-sections can be reached when the dielectric sphere is placed on the metallic substrate. For comparison, the measured sphere with  $r_o = 1 \mu\text{m}$  on a gold substrate, reaches an absorption cross-section of  $24 \mu\text{m}^2$  (Fig. 1 (b), dotted curve), at a wavelength of  $8.85 \mu\text{m}$  ( $\sim 1130 \text{ cm}^{-1}$ ), i.e within the target spectral region of radiative cooling ( $8\text{-}14 \mu\text{m}$ ), while a typical mid-IR plasmonic antenna of the same characteristic size has an absorption cross-section of  $18 \mu\text{m}^2$ , at a resonance

wavelength of  $7 \mu\text{m}$ .<sup>20</sup>

To gain further qualitative insight regarding the origin of the resonances observed in Figs. 1 (b)-(e) and to highlight any similarities or differences between the case of a sphere on a metallic substrate and a sphere in free space, we have also performed Mie theory calculations of the absorption cross-section of the measured spheres in vacuum (Figs. 2 (c)-(f)), which we illustrate below.

$\text{SiO}_2$  is a polar dielectric material supporting SPhP modes resulting from the coupling of the material's optical phonons with photons at mid-IR frequencies. These modes arise from the material's *Reststrahlen* band between the transverse and longitudinal optical phonon frequencies ( $\omega_{TO}$  and  $\omega_{LO}$ , respectively), in which the real part of the dielectric function is negative (see Fig. 2 (b)). Polar dielectric spheres exhibit transverse modes (for which  $\nabla \cdot \mathbf{E} = 0$ ) of three types: (i) low-frequency modes having frequency  $\omega \leq \omega_{TO}$ , where the real part of the sphere's dielectric function is positive ( $\epsilon' > 0$ ) (ii) high-frequency modes for which  $\omega \geq \omega_{LO}$ , and (iii) surface modes with frequencies that are intermediate between  $\omega_{TO}$  and  $\omega_{LO}$ , where  $\epsilon' < 0$  (see Fig. 2 (b)).<sup>33,34</sup>

Owing to its sub- $\lambda$  size, the sphere can couple directly to propagating light, resulting in radiative damping. In polar dielectric spheres, additional Ohmic losses arise from anharmonic processes, such as phonon-phonon and phonon-defect scattering.<sup>35-38</sup> Consequently, the transverse modes all have complex frequencies, and therefore, result in temporal decay of the sphere's time harmonic fields. Such modes are hence referred to as virtual modes.<sup>33,34</sup> However, in an optical experiment, the measured observables, such as the sphere's cross-sections, correspond to real frequencies.

The cross-sections of a sphere in free space, illuminated by a plane wave, can be calculated from the scattering coefficients given by Mie theory.<sup>39,40</sup> In this context, the fields are expanded in terms of multipoles, alternatively of the electric and magnetic type, given by the scattering coefficients  $a_l$  and  $b_l$  (see Supplementary Information, Eqs. 6 and 7), respectively, where  $l$  is the mode number. Hence,  $a_1$  and  $b_1$  correspond to the electric and magnetic

dipolar modes,  $a_2$  and  $b_2$  correspond to the electric and magnetic quadrupolar modes, and so on. The frequencies of the sphere's transverse virtual modes correspond to that of vanishing denominators of the real parts of the scattering coefficients  $a_l$  and  $b_l$  (see supplementary information, Section 2), thus, each virtual mode coincides with a peak in the sphere's cross-section spectrum.

Figs. 2 (c)-(f) show Mie theory calculations of the absorption cross-section corresponding to the measured spheres in vacuum (black curves, see Supplementary information Eq. 5), along with the individual contributions of the first few electric and magnetic modes (given by the coefficients  $a_l$  and  $b_l$ ) to the absorption cross-section in each case (colored curves). Data reported in ref.<sup>32</sup> were used for the dielectric constant of SiO<sub>2</sub> (Fig. 2 (b)). For  $r_o = 1 \mu\text{m}$ , a sharp resonance peak is observed in the total absorption cross-section between  $\omega_{TO}$  and  $\omega_{LO}$  (blue shaded region), near  $1130 \text{ cm}^{-1}$ . This peak corresponds to the spheres' surface mode, which represents the mid-IR phononic counterpart of plasmonic resonances characteristic of noble metals in the visible spectral range. In the quasi-electrostatic approximation, this mode's frequency coincides with the condition:  $\varepsilon' = -\epsilon_m(l+1)/l$  ( $\varepsilon'$  being the real part of the sphere's dielectric function, and  $\epsilon_m$  the permittivity of the surrounding medium),<sup>33</sup> for which  $l=1$  gives the frequency of the well-known Frohlich mode.<sup>41,42</sup> In addition to becoming predominant as the sphere size decreases,<sup>43</sup> the surface mode has been shown to be exclusively of electric nature.<sup>33</sup>

As evidenced by Fig. 2 (c), the dominant contribution to the surface mode peak in the smallest considered sphere, comes from the electric dipolar mode (cf. Fig. 2 (a)), hence, corresponding to the Frohlich mode, while as the sphere radius increases, contributions from higher order modes, such as the quadrupolar electric mode ( $a_2$ , blue curves), and the octupolar mode ( $a_3$ , turquoise curve), become more pronounced (see Fig. 2 (f)).

By comparing the calculated absorption cross-sections of the spheres with and without the gold substrate (Figs. 1 (b)-(e), and Figs. 2 (c)-(f), respectively), it is clear that the metallic substrate induces a large enhancement of the spheres' absorption cross-section. In particular,

for the smallest considered sphere, which mainly exhibits dipolar emission, the FEM simulation with the gold substrate shows an enhancement of the sphere's absorption cross-section above the unitary limit of  $3\lambda^2/8\pi$  (where  $\lambda$  is the resonance wavelength) for a resonant dipole in vacuum.<sup>44</sup> This limit corresponds to  $9.35 \mu\text{m}^2$  at  $1130 \text{ cm}^{-1}$ . As shown in the left inset of Fig. 1 (b), the presence of the gold substrate leads to a large electric field enhancement between the sphere and substrate, giving rise to increased local field absorption by the sphere. This increase is ultimately expressed in the large values of  $C_{abs}$  obtained in Figs. 1 (b)-(e) for the sphere on gold.

In contrast to a sphere in vacuum, the pronounced surface mode peak (between  $\omega_{TO}$  and  $\omega_{LO}$ ) is markedly absent in the thermal radiation spectra of a sphere on a gold substrate for  $r_o > 1$  (Figs. 1 (c)-(e)). As  $r_o$  increases above  $1 \mu\text{m}$ , the electric dipolar mode red-shifts towards  $\omega_{TO}$ , where the material absorbs resonantly (see Figs. 2 (d)-(f),  $a_1$ , magenta). The electric dipolar mode, thus, broadens due to material losses and increased radiative damping with increasing sphere size, and eventually splits into two peaks, one with frequency  $\omega < \omega_{TO}$ , and another with  $\omega_{TO} < \omega < \omega_{LO}$  (Figs. 2 (e) and (f), magenta curve). For spheres with diameters above  $2 \mu\text{m}$ , we also observe a major contribution to the radiation spectrum from the magnetic dipolar mode below  $\omega_{TO}$  (Figs. 2 (d)-(f), red curve). These electric and magnetic dipolar Mie modes correspond to the spheres' low-frequency transverse mode, which is predominant in the total absorption (equivalently, emission) spectrum of the sphere on gold. The emergence of these modes can be explained by the large real part of the dielectric constant of  $\text{SiO}_2$ ,  $\varepsilon'_{\text{SiO}_2}$ , just below  $\omega_{TO}$  (see Fig. 2 (b)). The magnetic modes in particular arise from the coupling of circular displacement currents of the electric field, with incoming radiation, when  $2r_o \sim \lambda/n$ ,<sup>1</sup> where  $n$  is the real part of the index of refraction of the sphere, and  $\lambda$  is the wavelength of incident light. It is also interesting to note that  $\varepsilon'_{\text{SiO}_2}$  is positive in this spectral region, while it is negative in the *Reststrahlen* band, which changes the nature of the observed resonances. In Figs. 1 (b)-(e) we can, thus, observe the transition from an absorption cross-section dominated by a phononic mode ( $r_o = 1 \mu\text{m}$ ,  $\varepsilon'_{\text{SiO}_2} < 0$ , Fig. 1 (b))

to that dominated by electric and magnetic dipolar geometrical Mie modes ( $r_o > 1 \mu\text{m}$ ,  $\epsilon'_{\text{SiO}_2} > 0$ , Figs. 1 (c)-(e)). These results also show that a sphere radius of  $1.5 \mu\text{m}$  can be considered as a cross-over value between the two observed absorption regimes.

Figs. 2 (c)-(f) also show a peak in the absorption spectrum around  $800 \text{ cm}^{-1}$ , which is invariant with respect to sphere size. This peak results from the bulk absorption of  $\text{SiO}_2$ , due to the presence of a local maximum in the imaginary part of the dielectric function at this frequency (see Fig. 2 (b)). Note that the high-frequency transverse modes ( $\omega \geq \omega_{LO}$ ) will not be discussed here as they arise at very large frequencies (several times  $\omega_{TO}$ ) for the sphere sizes considered here,<sup>35</sup> which lie outside of the spectral range accessible by our experiment. Overall, the gold substrate leads to an enhancement of the spheres' low-frequency mode— which is dominated by electric and magnetic dipolar Mie modes— over the spheres' surface mode (cf. Figs. 1 (c)-(e) with Figs. 2 (d)-(f)). A slight red-shift in the spheres' resonance peaks is also observed in the presence of the substrate. This is a signature of the interaction with the gold substrate.<sup>45-47</sup> In the mid-IR the Au substrate acts as a mirror. When a sphere is placed on top of it, it might look, at first glance, as a dimer of two stacked spheres. Yet, when considering near-field interactions, the situation is dramatically different due to the  $\pi$  phase-shift of the in-plane electric field component, induced by the metallic surface, as sketched in Fig. 3 (a). For spheres that act as dipoles very close to the surface in the quasi-electrostatic limit,<sup>48</sup> the effect of the substrate is described by the sphere's interaction with the induced image charges of opposite sign. The observed red-shift is a direct consequence of the attraction between the sphere and its image.

As presented in Figs. 2 (d) and (e), a large contribution to the surface mode for the  $1.5$  and  $2 \mu\text{m}$  radius spheres, in the absence of the substrate, comes from the electric quadrupolar mode ( $a_2$ , blue curve), while the sphere's low frequency mode arises mainly due to the electric dipolar Mie mode ( $a_1$ , magenta curve). Fig. 3 (b) (top panel) shows the simulated electric field enhancement map calculated at the surface mode frequency ( $1130 \text{ cm}^{-1}$ ), which indeed reveals a distribution expected for a quadrupolar mode. When the gold substrate is

introduced, the presence of charges near the bottom of the sphere, that are in close proximity to the induced image charges for this mode (Fig. 3 (a)), leads to a strong field enhancement and confinement between the sphere and substrate (Fig. 3 (b), bottom panel). This leads to an increased cross-section with respect to the isolated sphere case, as well as a distortion of the mode's field distribution, resulting in a quasi-total suppression of the sphere's surface mode, in good agreement with the absence of the peak near  $1130 \text{ cm}^{-1}$  in Figs. 1 (c) and (d).

For a radius of  $2.5 \text{ }\mu\text{m}$ , the measurements and simulations show that the surface mode is again observable in the presence of the substrate (Fig. 1 (e)). When the sphere is that large, the sphere/image pair, which was heretofore of sub- $\lambda$  dimensions, becomes comparable to the wavelength of excited thermal radiation (equivalently to the wavelength of incident radiation in the calculations, since emissivity is equal to absorptivity). The behavior in this case is no longer dominated by quasi-electrostatic interactions, and the quadrupolar mode is found to be less degraded on the gold substrate, for normal incidence, compared to the case of spheres with smaller diameters (see Fig. 3 (d), top panel). Higher order modes, such as the octupolar mode (see Fig. 2 (f), turquoise curve), are also excited and contribute to the sphere's surface mode for this large size. Consequently, the surface mode is still observable near  $1130 \text{ cm}^{-1}$  in the measured thermal radiation spectrum in this case (Fig. 1 (e)), in spite of the perturbation induced by the metallic substrate.

In addition to inducing image charges of the sphere, the gold substrate breaks the spherical symmetry so that the resonances of the sphere become dependent on the properties of the incident electric field, i.e on the field's polarization and angle of incidence.<sup>49</sup> By the principle of reciprocity, this means that the far-field thermal radiation spectrum of a sphere on a substrate will depend on the angle at which it is probed – determined by the reflective objective in our measurements, which is not the case for a sphere in vacuum or surrounded by a homogeneous dielectric medium.

To elucidate this point, and to study the influence of angle of incidence on the sphere's virtual

modes, we show in Fig. 3 (c) the values of the absorption cross-section, obtained from FEM simulations of a sphere with  $r_o = 2.5 \mu\text{m}$ , on a gold substrate, for various angles of incidence  $\theta$  (from  $0^\circ$  to  $30^\circ$ ), at the frequencies of the surface mode ( $1130 \text{ cm}^{-1}$ ) and low-frequency mode ( $1000 \text{ cm}^{-1}$ ) (see Fig. S1 (b), Supplementary Information, for full spectra). It is found that the surface mode in this case is greatly influenced by the angle of incidence, whereas the low-frequency virtual mode, with its characteristic dipolar emission, is unaffected (see Fig. 3 (c), blue circles). The surface mode peak exhibits a significant contribution to the total absorption cross-section, at normal incidence, for a sphere with  $r_o = 2.5 \mu\text{m}$ , on gold (see Fig. S1 (b)). Nevertheless, its contribution decreases with increasing angle, and disappears completely at  $30^\circ$  (Fig. S1 (b), green curve). At large angles, the asymmetry of the induced charges around the sphere results in a reduction of the sphere’s surface mode peak. This is corroborated by the field plot in Fig. 3 (d) (bottom panel), which shows a distorted field distribution around the sphere at  $30^\circ$  incidence, near the surface mode frequency.

In order to show that the unique spectral features exhibited by the studied sub- $\lambda$   $\text{SiO}_2$  spheres originate from the excitation of virtual SPhP modes in combination with geometrical Mie modes, we measured the thermal radiation of a sub- $\lambda$  PTFE sphere, with  $r_o = 1.5 \mu\text{m}$ , placed on a gold substrate (Fig. 4 (a)). PTFE is a polymer with high absorption in the mid-IR and no *Reststrahlen* band (see Fig. 4 (b), inset). The measurement and corresponding simulation reveal two peaks near  $1159$  and  $1220 \text{ cm}^{-1}$ , akin to the bulk absorption peaks of PTFE (cf. Fig. 4 (b), inset). Further, Mie theory calculations of a PTFE sphere in vacuum with variable radius  $r_o$  (Fig. 4 (b)) show that the absorption spectrum is invariant with respect to sphere size.

The absorption length of mid-IR photons in PTFE, at its absorption peaks, is around  $1 \mu\text{m}$  (calculated as  $\lambda/4\pi\kappa$ , where  $\kappa$  is the imaginary part of the index of refraction). For a sub- $\lambda$  PTFE sphere to be resonant at mid-IR frequencies, its characteristic size should thus be smaller than  $1 \mu\text{m}$ . This is too small to produce size-dependent absorption resonances at mid-IR wavelengths. Bulk features, therefore, dominate the absorption spectrum of such lossy

spheres. By contrast, the investigated SiO<sub>2</sub> spheres display phononic and size dependent resonances, in spite of an absorption length of  $\sim 0.4 \mu\text{m}$  near the surface mode frequency. It has been shown that the absorption efficiency ( $C_{abs}/\pi r_o^2$ ) of lossy spheres, such as the PTFE spheres considered here, is limited to  $\sim 3/2$  for large radii.<sup>51</sup> This is consistent with our calculations of the absorption efficiency of large PTFE spheres in vacuum based on Mie theory (see Fig. 4 (b), green and magenta curves). For a PTFE sphere on a gold substrate (Fig. 4 (a)), the absorption efficiency reaches more than twice this value due to the presence of the image sphere.

## Conclusions

In summary, we have characterized the far-field thermal radiation of single sub- $\lambda$  SiO<sub>2</sub> spheres on a gold substrate, using IR-SMS. The measurements, and corresponding analysis based on FEM simulations and rigorous Mie theory calculations, revealed that the dielectric and geometrical properties of the investigated sub- $\lambda$  SiO<sub>2</sub> spheres allow the excitation of both phononic and geometrical Mie resonances of the electric and magnetic type. The phononic resonance observed in the measured single polar dielectric spheres, is a direct analogue to plasmonic resonances exhibited by noble metals in the visible spectral range. The geometrical Mie modes, on the other hand, are equivalent to those prevalent in high-refractive-index dielectric spheres, such as silicon nanospheres, in the visible and near-IR.<sup>9</sup> The observation of both types of resonances is a direct consequence of the fact that SiO<sub>2</sub> is a polar dielectric material, whose real part of its dielectric function can, thus, be either positive, as in dielectric materials, or negative as in metals, depending on the optical frequency. Through sweeping the measured sphere size, a transition from a phononic-mode-dominated to a Mie-mode-dominated absorption spectrum was observed. Further, the combination of the resonant dielectric microsphere and the metallic substrate was shown to result in a large enhancement of the sphere's absorption cross-section, above the unitary limit achievable by a resonant

dipole in vacuum. This arises due to a substantial enhancement of the local field between the sphere and substrate, as a consequence of the interaction of the sphere with its induced image in the substrate. Lastly, measurement of the far-field thermal radiation of a single sub- $\lambda$  PTFE sphere on a gold substrate, along with Mie theory calculations of absorption efficiency of PTFE spheres in vacuum, showed that contrary to  $\text{SiO}_2$  spheres, the absorption spectrum of such lossy dielectric spheres, which are SPhP-inactive, is dominated by bulk absorption.

Our study of the mid-IR far-field thermal radiation of single dielectric spheres on a metallic substrate offers new insights into the geometrical and electromagnetic degrees of freedom that allow the engineering of the mid-IR absorption and radiation properties of single dielectric spheres. This will allow, for instance, the design and optimization of systems based on dielectric spheres on a metallic substrate that achieve efficient radiative cooling properties, i.e. a large emissivity only in the infrared atmospheric window (predominantly between 8 and 14  $\mu\text{m}$ ). Moreover, the large field confinement and enhancement observed between the resonant dielectric sphere and metallic substrate could be of interest for bio-detection applications, such as surface enhanced infrared absorption spectroscopy.

## Acknowledgement

This work has received financial support from Agence Nationale de la Recherche (ANR-10-LABX-24, ANR-10-IDEX-0001-02PSL\*, ANR-21-CE30-0030, and ANR-16-CE09-0012) .

## Supporting Information Available

A supplementary information document is available for this manuscript. The supplementary information includes the following:

- Methods: Sample preparation and Finite element method (FEM) simulations

- Virtual modes and sphere cross-sections
- Angle resolved FEM spectra of a sphere on gold

## References

- (1) Kuznetsov, A. I.; Miroshnichenko, A. E.; Brongersma, M. L.; Kivshar, Y. S.; Luk'yanchuk, B. Optically resonant dielectric nanostructures. *Science* **2016**, *354*.
- (2) Bidault, S.; Mivelle, M.; Bonod, N. Dielectric nanoantennas to manipulate solid-state light emission. *J. Appl. Phys.* **2019**, *126*, 094104.
- (3) Schmidt, M. K.; Esteban, R.; Sáenz, J.; Suárez-Lacalle, I.; Mackowski, S.; Aizpurua, J. Dielectric antennas-a suitable platform for controlling magnetic dipolar emission. *Opt. Express* **2012**, *20*, 13636–13650.
- (4) Krasnok, A. E.; Miroshnichenko, A. E.; Belov, P. A.; Kivshar, Y. S. All-dielectric optical nanoantennas. *Opt. Express* **2012**, *20*, 20599–20604.
- (5) Rolly, B.; Stout, B.; Bonod, N. Boosting the directivity of optical antennas with magnetic and electric dipolar resonant particles. *Opt. Express* **2012**, *20*, 20376–20386.
- (6) Van de Groep, J.; Polman, A. Designing dielectric resonators on substrates: Combining magnetic and electric resonances. *Opt. Express* **2013**, *21*, 26285–26302.
- (7) Staude, I.; Miroshnichenko, A. E.; Decker, M.; Fofang, N. T.; Liu, S.; Gonzales, E.; Dominguez, J.; Luk, T. S.; Neshev, D. N.; Brener, I., et al. Tailoring directional scattering through magnetic and electric resonances in subwavelength silicon nanodisks. *ACS Nano* **2013**, *7*, 7824–7832.
- (8) Butakov, N. A.; Schuller, J. A. Designing multipolar resonances in dielectric metamaterials. *Sci. Rep.* **2016**, *6*, 1–8.

- (9) García-Etxarri, A.; Gómez-Medina, R.; Froufe-Pérez, L. S.; López, C.; Chantada, L.; Scheffold, F.; Aizpurua, J.; Nieto-Vesperinas, M.; Sáenz, J. J. Strong magnetic response of submicron silicon particles in the infrared. *Opt. Express* **2011**, *19*, 4815–4826.
- (10) Miroshnichenko, A. E.; Evlyukhin, A. B.; Kivshar, Y. S.; Chichkov, B. N. Substrate-induced resonant magnetoelectric effects for dielectric nanoparticles. *ACS Photonics* **2015**, *2*, 1423–1428.
- (11) Sugimoto, H.; Fujii, M. Broadband dielectric–metal hybrid nanoantenna: Silicon nanoparticle on a mirror. *ACS Photonics* **2018**, *5*, 1986–1993.
- (12) Zhai, Y.; Ma, Y.; David, S. N.; Zhao, D.; Lou, R.; Tan, G.; Yang, R.; Yin, X. Scalable-manufactured randomized glass-polymer hybrid metamaterial for daytime radiative cooling. *Science* **2017**, *355*, 1062–1066.
- (13) Liu, C.; Hu, N.; Li, Q.; Qiu, M. Metal-dielectric hybrid structure for radiative cooling. *J. Phys. Conf. Ser.* 2018; p 012003.
- (14) Jaramillo-Fernandez, J.; Whitworth, G. L.; Pariente, J. A.; Blanco, A.; Garcia, P. D.; Lopez, C.; Sotomayor-Torres, C. M. A Self-Assembled 2D Thermofunctional Material for Radiative Cooling. *Small* **2019**, *15*, 1905290.
- (15) Feng, J.; Santamouris, M.; Gao, K. The radiative cooling efficiency of silica sphere embedded polymethylpentene (TPX) systems. *Sol. Energy Mater.* **2020**, *215*, 110671.
- (16) Chen, M.; Pang, D.; Chen, X.; Yan, H. Investigating the effective radiative cooling performance of random dielectric microsphere coatings. *Int. J. Heat Mass Transf.* **2021**, *173*, 121263.
- (17) Xiang, B.; Zhang, R.; Luo, Y.; Zhang, S.; Xu, L.; Min, H.; Tang, S.; Meng, X. 3D porous polymer film with designed pore architecture and auto-deposited SiO<sub>2</sub> for highly efficient passive radiative cooling. *Nano Energy* **2021**, *81*, 105600.

- (18) Wheeler, M. S.; Aitchison, J. S.; Mojahedi, M. Coated nonmagnetic spheres with a negative index of refraction at infrared frequencies. *Phys. Rev. B* **2006**, *73*, 045105.
- (19) Wheeler, M. S.; Aitchison, J. S.; Chen, J. I.; Ozin, G. A.; Mojahedi, M. Infrared magnetic response in a random silicon carbide micropowder. *Phys. Rev. B* **2009**, *79*, 073103.
- (20) Li, C.; Krachmalnicoff, V.; Bouchon, P.; Jaeck, J.; Bardou, N.; Haidar, R.; De Wilde, Y. Near-field and far-field thermal emission of an individual patch nanoantenna. *Phys. Rev. Lett.* **2018**, *121*, 243901.
- (21) Abou-Hamdan, L.; Li, C.; Haidar, R.; Krachmalnicoff, V.; Bouchon, P.; De Wilde, Y. Hybrid modes in a single thermally excited asymmetric dimer antenna. *Opt. Lett.* **2021**, *46*, 981–984.
- (22) Revercomb, H. E.; Buijs, H.; Howell, H. B.; LaPorte, D. D.; Smith, W. L.; Sromovsky, L. Radiometric calibration of IR Fourier transform spectrometers: solution to a problem with the High-Resolution Interferometer Sounder. *Appl. Opt.* **1988**, *27*, 3210–3218.
- (23) Kirchhoff, G. I. On the relation between the radiating and absorbing powers of different bodies for light and heat. *Lond. Edinb. Dublin Philos. Mag. J. Sci.* **1860**, *20*, 1–21.
- (24) Kattawar, G.; Eisner, M. Radiation from a homogeneous isothermal sphere. *Appl. Opt.* **1970**, *9*, 2685–2690.
- (25) Kallel, H.; Doumouro, J.; Krachmalnicoff, V.; De Wilde, Y.; Joulain, K. Thermal emission from a single glass fiber. *J. Quant. Spectrosc. Radiat. Transf.* **2019**, *236*, 106598.
- (26) Doumouro, J.; Perros, E.; Dodu, A.; Rahbany, N.; Leprat, D.; Krachmalnicoff, V.; Carminati, R.; Poirier, W.; De Wilde, Y. Quantitative measurement of the thermal

- contact resistance between a glass microsphere and a plate. *Phys. Rev. Appl.* **2021**, *15*, 014063.
- (27) Joulain, K.; Ben-Abdallah, P.; Chapuis, P.-O.; De Wilde, Y.; Babuty, A.; Henkel, C. Strong tip-sample coupling in thermal radiation scanning tunneling microscopy. *J. Quant. Spectrosc. Radiat. Transf.* **2014**, *136*, 1–15.
- (28) Herz, F.; Biehs, S.-A. Dipole model for far-field thermal emission of a nanoparticle above a planar substrate. *J. Quant. Spectrosc. Radiat. Transf.* **2021**, *266*, 107572.
- (29) Bobbert, P.; Vlieger, J. Light scattering by a sphere on a substrate. *Phys. A: Stat. Mech. Appl.* **1986**, *137*, 209–242.
- (30) Videen, G. Light scattering from a sphere on or near a surface. *J. Opt. Soc. Am. A: Opt. Image Sci. Vis.* **1991**, *8*, 483–489.
- (31) Herz, F.; Biehs, S.-A. Generalized coupled dipole method for thermal far-field radiation. *Phys. Rev. B* **2022**, *105*, 205422.
- (32) Palik, E. D. *Handbook of optical constants of solids*; Academic press, 1998; Vol. 3.
- (33) Fuchs, R.; Kliever, K. Optical modes of vibration in an ionic crystal sphere. *J. Opt. Soc. Am.* **1968**, *58*, 319–330.
- (34) Kliever, K.; Fuchs, R. *Theory of dynamical properties of dielectric surfaces*; Wiley, UK, 1974; Vol. 27.
- (35) Klemens, P. Anharmonic decay of optical phonons. *Phys. Rev.* **1966**, *148*, 845.
- (36) Balkanski, M.; Wallis, R.; Haro, E. Anharmonic effects in light scattering due to optical phonons in silicon. *Phys. Rev. B* **1983**, *28*, 1928.
- (37) Maris, H. J. Phonon propagation with isotope scattering and spontaneous anharmonic decay. *Phys. Rev. B* **1990**, *41*, 9736.

- (38) Maradudin, A.; Califano, S. Theory of anharmonic processes in crystals with isotopic impurities. *Phys. Rev. B* **1993**, *48*, 12628.
- (39) Mie, G. Beiträge zur Optik trüber Medien, speziell kolloidaler Metallösungen. *Ann. Phys.* **1908**, *330*, 377–445.
- (40) Bohren, C. F.; Huffman, D. R. *Absorption and scattering of light by small particles*; John Wiley & Sons, 2008; p 103.
- (41) Frohlich, H. *Theory of Dielectrics: Oxford Univ*; 1949; pp 149–155.
- (42) Ruppin, R. Thermal fluctuations and Raman scattering in small spherical crystals. *J. Phys. C: Solid State Phys.* **1975**, *8*, 1969.
- (43) Hayashi, S. Optical study of electromagnetic surface modes in microcrystals. *Jpn. J. Appl. Phys.* **1984**, *23*, 665.
- (44) Striebel, M.; Wrachtrup, J.; Gerhardt, I. Absorption and extinction cross sections and photon streamlines in the optical near-field. *Sci. Rep.* **2017**, *7*, 1–13.
- (45) Ruppin, R. Surface modes and optical absorption of a small sphere above a substrate. *Surf. Sci.* **1983**, *127*, 108–118.
- (46) Takemori, T.; Inoue, M.; Ohtaka, K. Optical response of a sphere coupled to a metal substrate. *J. Phys. Soc. Japan* **1987**, *56*, 1587–1602.
- (47) Ruppin, R. Optical absorption by a small sphere above a substrate with inclusion of nonlocal effects. *Phys. Rev. B* **1992**, *45*, 11209.
- (48) Knoll, B.; Keilmann, F. Enhanced dielectric contrast in scattering-type scanning near-field optical microscopy. *Opt. Commun.* **2000**, *182*, 321–328.
- (49) Lermé, J.; Bonnet, C.; Broyer, M.; Cottancin, E.; Manchon, D.; Pellarin, M. Optical properties of a particle above a dielectric interface: cross sections, benchmark calcu-

- lations, and analysis of the intrinsic substrate effects. *J. Phys. Chem. C* **2013**, *117*, 6383–6398.
- (50) Korte, E. H.; Röseler, A. Infrared reststrahlen revisited: commonly disregarded optical details related to  $n < 1$ . *Anal. Bioanal. Chem.* **2005**, *382*, 1987–1992.
- (51) Tribelsky, M. I.; Miroshnichenko, A. E. Giant in-particle field concentration and Fano resonances at light scattering by high-refractive-index particles. *Phys. Rev. A* **2016**, *93*, 053837.

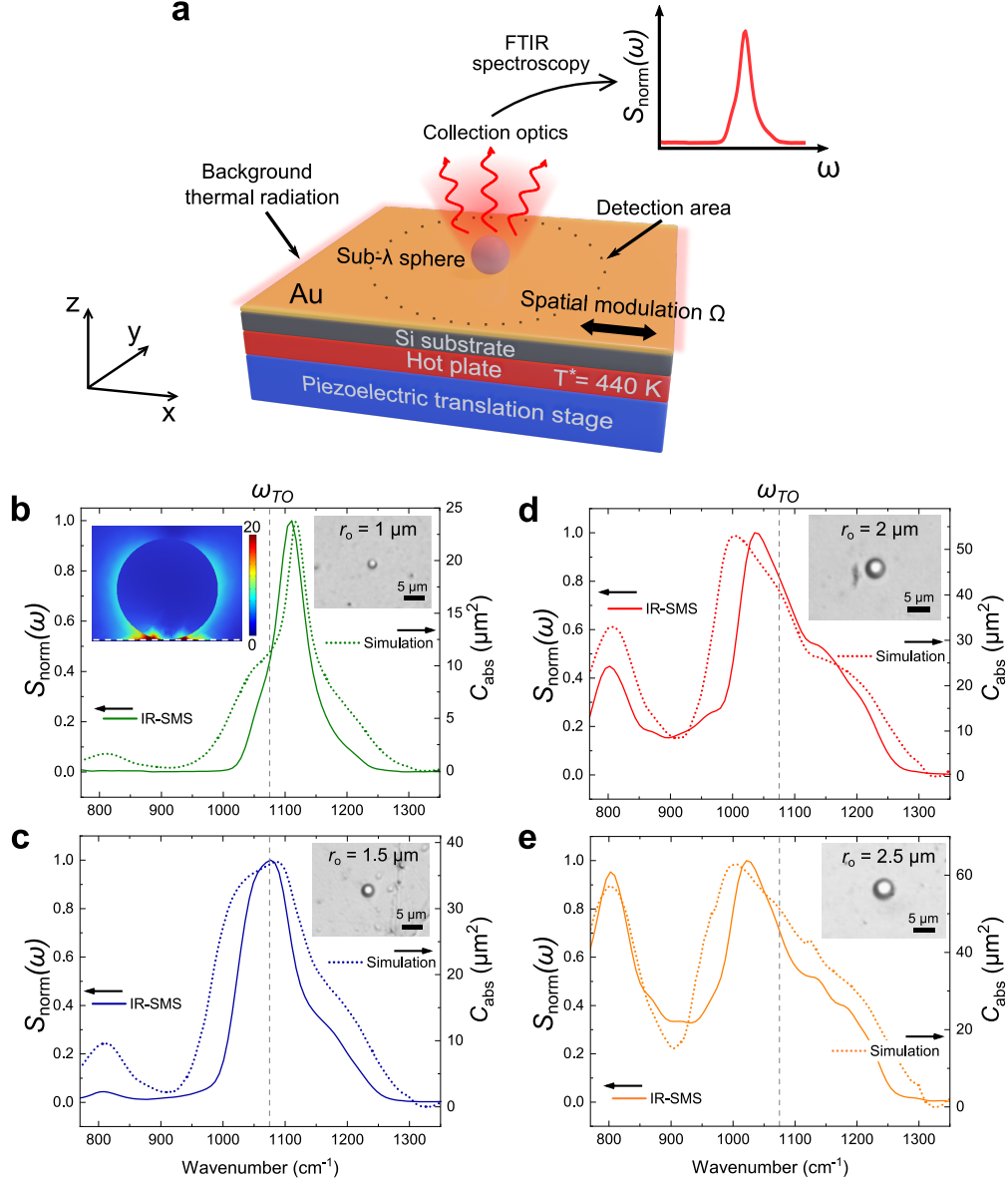


Figure 1: (a) Illustration of the IR-SMS technique for the measurement of far-field thermal radiation of single sub- $\lambda$  resonators. (b), (c), (d), and (e) Measured IR-SMS thermal radiation spectra of single sub- $\lambda$  SiO<sub>2</sub> spheres on a gold substrate (solid curves, left axis, normalized to 1), along with FEM simulations of their absorption cross-section ( $C_{\text{abs}}$ , dotted curves, right axis), for  $r_o = 1, 1.5, 2,$  and  $2.5 \mu\text{m}$ . The dashed vertical line marks the spectral position of the transverse optical phonon resonance frequency ( $\omega_{TO}$ ) in SiO<sub>2</sub>. The plotted FEM spectra are an average of  $C_{\text{abs}}$  of the sphere on gold, simulated with unpolarized light, incident at various angles from  $10$  to  $30^\circ$  (see supplementary information, subsection 1.2.1 for simulation details). The right insets show visible microscope images of the measured spheres, taken using a  $\times 50$ ,  $\text{NA}=0.55$  visible objective. The left inset of panel (b) shows the simulated electric field enhancement  $|E|/|E_o|$ , where  $|E_o|$  is the amplitude of the incident electric field (incident at  $20^\circ$  from the normal), calculated at the peak of the absorption cross-section, in the  $xz$ -plane for a sphere with  $r_o = 1 \mu\text{m}$  on a gold surface. The white dashed line indicates the intersection of the gold substrate with the sphere.

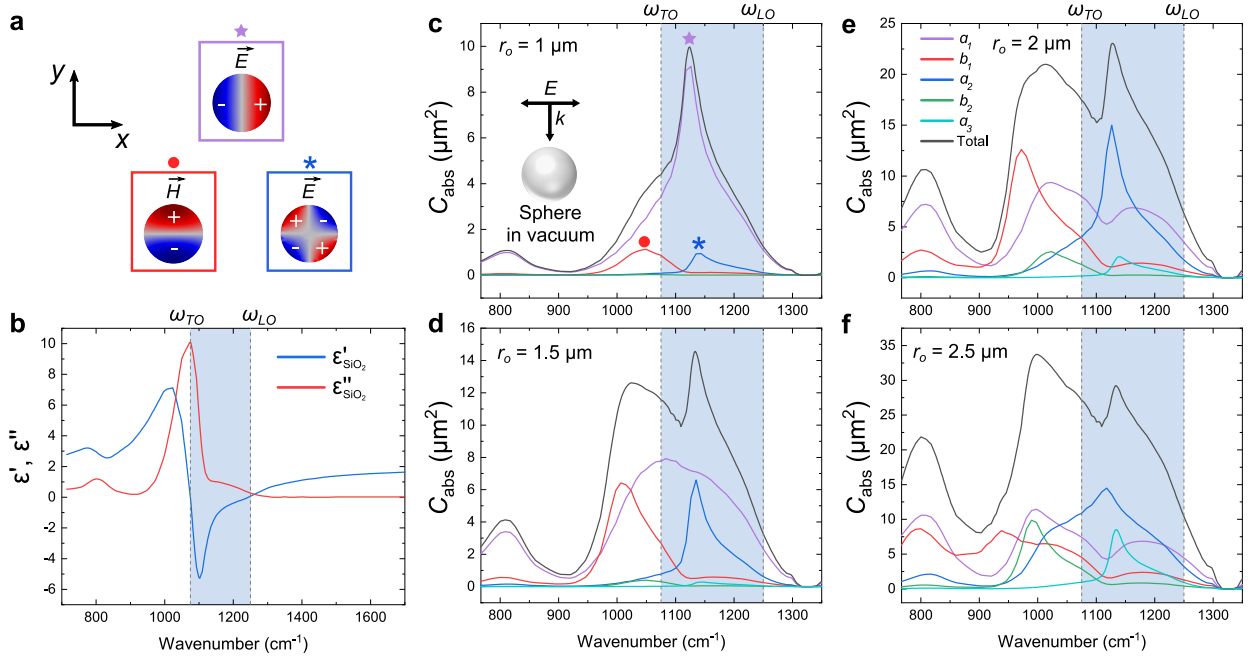


Figure 2: (a) Simulated distribution of the electric ( $\vec{E}$ ) and magnetic ( $\vec{H}$ ) fields inside an SiO<sub>2</sub> sphere of radius  $r_o = 1 \mu\text{m}$ , in vacuum (for electric field incident into the page and polarized along x) at the maxima of the peaks indicated by the markers in panel (c). They correspond to: the electric dipole (star), magnetic dipole (circle), and electric quadrupole (asterisk) modes of the sphere. (b) Real ( $\epsilon'_{\text{SiO}_2}$ ), and imaginary ( $\epsilon''_{\text{SiO}_2}$ ) parts of the dielectric function of SiO<sub>2</sub>, taken from ref.<sup>32</sup> The blue shaded region indicates the *Reststrahlen* band between the transverse ( $\omega_{TO}$ ) and the longitudinal ( $\omega_{LO}$ ) optical phonon frequencies in which the real part of the dielectric function is negative. (c), (d), (e) and (f) Mie theory calculation of the absorption cross-section of SiO<sub>2</sub> spheres in vacuum, of radii  $r_o = 1, 1.5, 2,$  and  $2.5 \mu\text{m}$ , along with the individual contributions of the first few electric and magnetic modes to the absorption cross-section.

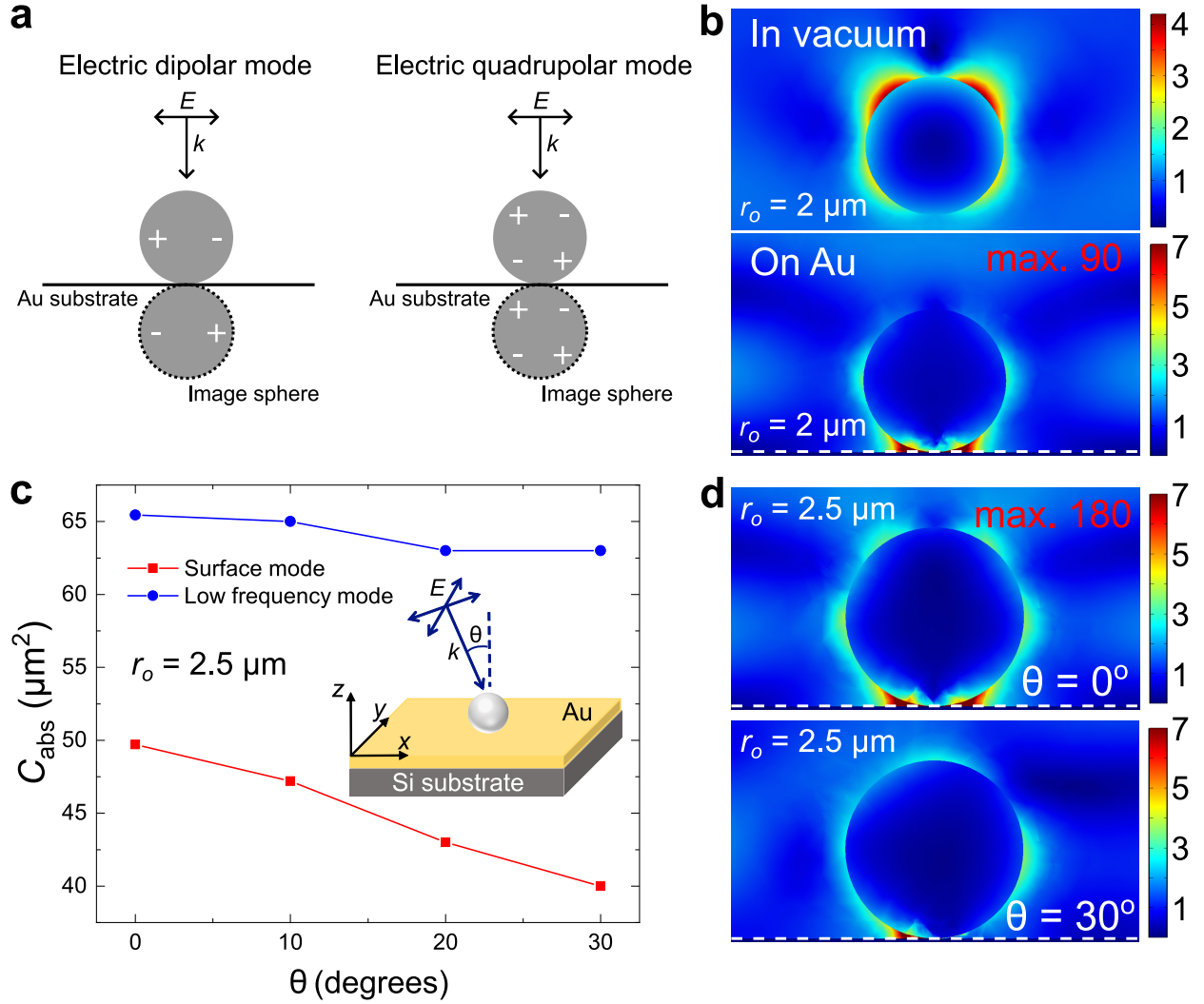


Figure 3: (a) Sketch of the sphere and image sphere charges, induced by the gold substrate, for the electric dipolar and quadrupolar modes. (b) Simulated electric field enhancement ( $|E|/|E_o|$ ), calculated at the electric quadrupolar mode frequency in the  $xz$ -plane for a sphere with  $r_o = 2 \mu\text{m}$  in vacuum (top panel), and on an Au substrate (bottom panel), for normal incidence,  $\theta = 0^\circ$ . Due to the large field enhancement between the sphere and substrate, the color bar in the bottom panel is scaled to reveal the field features. The value in the top right inset in red indicates the maximal calculated field enhancement near the point of intersection between the sphere and the gold substrate. The white dashed line indicates the intersection of the gold substrate with the sphere. (c) Calculated absorption cross-section at the surface and low frequency virtual modes of an  $\text{SiO}_2$  sphere with  $r_o = 2.5 \mu\text{m}$  on Au, for unpolarized light incident at various angles  $\theta$ , as sketched in the inset. (d) Electric field enhancement plots of an  $\text{SiO}_2$  sphere with  $r_o = 2.5 \mu\text{m}$  on gold, for  $\theta = 0^\circ$  and  $\theta = 30^\circ$ .

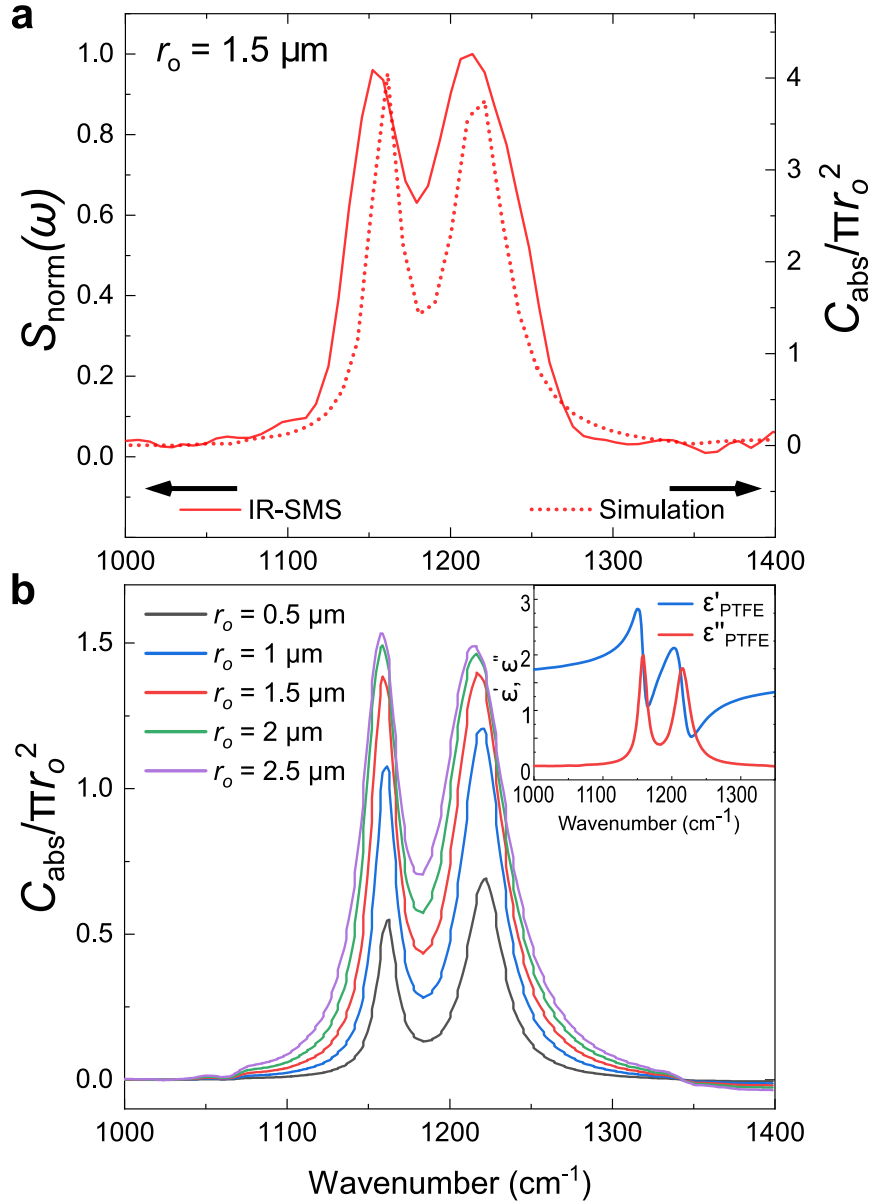


Figure 4: (a) Measured thermal radiation spectrum of a single PTFE sphere with  $r_o = 1.5 \mu\text{m}$  on a gold substrate (solid curve, left axis) and its corresponding simulated absorption efficiency ( $C_{\text{abs}}/\pi r_o^2$ , dotted curve, right axis) for unpolarized light averaged over various angles of incidence from  $10$  to  $30^\circ$  from the normal. (b) Mie theory calculation of the absorption efficiency of PTFE spheres, in vacuum, of various radii  $r_o$ . The inset shows the real ( $\epsilon'_{\text{PTFE}}$ ) and imaginary parts ( $\epsilon''_{\text{PTFE}}$ ) of the dielectric function of PTFE, taken from ref.<sup>50</sup>

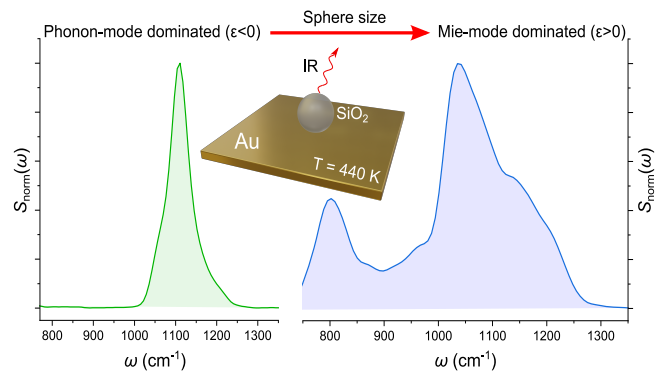


Figure 5: Graphical table of contents (TOC). Size: 8.47cm x 4.76cm